Photoresponsive and Polarization-Sensitive Structural Colors from Cellulose/Liquid Crystal Nanophotonic Structures

Prasaanth Ravi Anusuyadevi, Ravi Shanker, Yuxiao Cui, Anastasia V. Riazanova, Mikael Järn, Magnus P. Jonsson,* and Anna J. Svagan*

Cellulose nanocrystals (CNCs) possess the ability to form helical periodic structures that generate structural colors. Due to the helicity, such self-assembled cellulose structures preferentially reflect left-handed circularly polarized light of certain colors, while they remain transparent to right-handed circularly polarized light. This study shows that combination with a liquid crystal enables modulation of the optical response to obtain light reflection of both handedness but with reversed spectral profiles. As a result, the nanophotonic systems provide vibrant structural colors that are tunable via the incident light polarization. The results are attributed to the liquid crystal aligning on the CNC/glucose film, to form a birefringent layer that twists the incident light polarization before interaction with the chiral cellulose nanocomposite. Using a photoresponsive liquid crystal, this effect can further be turned off by exposure to UV light, which switches the nematic liquid crystal into a nonbirefringent isotropic phase. The study highlights the potential of hybrid cellulose systems to create self-assembled yet advanced photoresponsive and polarization-tunable nanophotonics.

1. Introduction

Structural coloration observed in plants and animals has several practical functions, ranging from signaling[1] and survival[2]

Dr. P. R. Anusuyadevi, Dr. Y. Cui, Dr. A. V. Riazanova, Dr. A. J. Svagan
Department of Fibre and Polymer Technology
Royal Institute of Technology (KTH)
Stockholm SE-100 44, Sweden
E-mail: svagan@kth.se
Dr. R. Shanker, Dr. M. P. Jonsson
Laboratory of Organic Electronics, Department of Science and Technology
Wallenberg Wood Science Center
Linköping University
Norrköping SE-601 74, Sweden
E-mail: magnus.jonsson@liu.se
Dr. M. Järn
Materials and Surface Design
RISE Research Institutes of Sweden
Stockholm SE-114 28, Sweden

to reproduction[3] and enhanced photosynthetic efficiency.[4] Such structural colors result from light interference in periodic arrangements of micro- or nanometer scaled structures found in these organisms. For example, the color of certain leaves and fruit shells originate from an ordered cholesteric structure based on cellulose microfibrils.[5] Replicating such chiral nematic structures using biological building blocks[6] is highly attractive to achieve sustainable, low-cost, nonfading, and nontoxic structural colors.[7] Bioinspired structural colors can be accomplished using cellulose nanocrystals (CNCs),[8] as these are capable of self-assembling into solid state films with chiral nematic structures, even in the presence of additional polymers or small molecular species.[9,10] Inclusion of supplementary compounds enables control of the cholesteric pitch, p (the distance of a full-turn period), and thereby wavelength-tuning of the structural colors. In this study, glucose was used to modulate the cholesteric pitch. Inclusion of glucose is advantageous because it has previously been shown to render CNC-templated inorganic photonic films flexible and crack-free.[10,11]

An interesting feature of chiral CNC-based nanocomposite films is that they only reflect light that has the same circularly polarized handedness as the film itself. Hence, left-handed CNC-films selectively reflect left-handed circularly polarized (LCP) light, while right-handed circularly polarized (RCP) light is transmitted through the film. Additionally, such films typically exhibit microscale domains with different periodicities, which results in a (finite) range of structural color combinations within a small area or along the thickness of the same film.[12,13] While such films can provide clear macroscopic dominating colors, the presence of the microscale color variations opens additional opportunities. Recent research has explored the combination of CNC films with other functional materials. As example, Fernandes et al. infiltrated a birefringent liquid crystal into the gaps and cracks of a pure CNC film with two different colors (green and orange) along the film's thickness, which resulted in reflection of light with orange color in RCP and green color in LCP.[12]

In this study, we report a simple and general strategy for achieving photoresponsive cellulose-based nanophotonic structures that can alter between two reflected structural colors. The
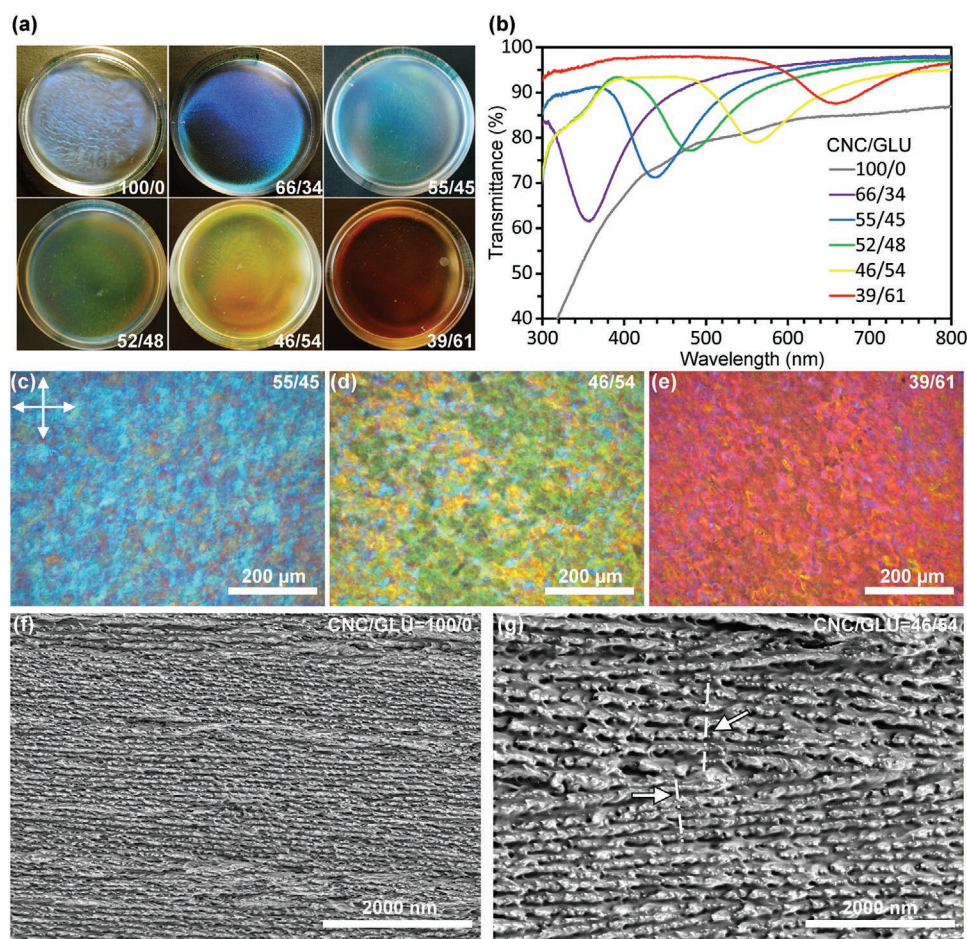
**ADVANCED
SCIENCE NEWS**
www.advancedsciencenews.com

**ADVANCED
MATERIALS**
www.advmat.de

Figure 1. CNC/GLU films. a) Photographs showing the structural colors of CNC/GLU films (6 cm in diameter) with different weight percentage (wt%) compositions (CNC/GLU = 100/0, 66/34, 55/45, 52/48, 46/54 or 39/61). b) UV–vis transmission spectra of different CNC/GLU films. c–e) Films observed between crossed polarizers in reflectance mode revealing the pixelated colors of each nanocomposite. f–g) SEM images of cross-sections of a neat CNC film (CNC/GLU = 100/0) and a nanocomposite film (46/54). The pitch increased with glucose content. The arrows in (g) point to the (different) tilts of the helical axis.

nanophotonic structure comprises structurally colored CNC/glucose (GLU) films topped with a UV-light-responsive birefringent LC layer. The results are discussed with respect to the multicolor feature of differently colored CNC/GLU films (violet, blue, green, yellow, and red) and the films' microstructure, molecular organization and interactions with the nematic liquid crystal phase residing on top of the films.

2. Results and Discussion

CNC/GLU films with different iridescent colors were attained by preparing films with different weight percentage (wt%) of glucose content (**Figure 1**a; see also the Supporting Information for experimental details). The films reflected structural colors that gradually redshifted with increasing glucose content, manifested as distinct dips in their transmission spectra (Figure 1b). All samples exhibited relatively broad transmission dips. As example, the dip of the yellow film (CNC/GLU = 46/54) spanned between ≈480–700 nm, which includes wavelengths of green, yellow and red colors within the same film. Figure 1c–e presents

polarized optical microscopy (POM) images in reflectance mode for the three primary color nanocomposite films (also see Figure S1, Supporting Information). Interestingly, even though each film had a single macroscopic dominating color, visualization of the films under crossed polarizers revealed a microscopic pixelated structural color palette. The detailed composition of the subcolors also varied between different areas of the films, as exemplified in Figure S2 of the Supporting Information for the blue film, showing areas containing different amounts of green features. Such digitalized colors, within the same film, result from a discrepancy in the cholesteric pitch (p),[14] and potentially a change in the tilt of the helical axis,[13] within different parts of the film (see the so-called fingerprint textures[15] in Figure S3, Supporting Information). Indeed, this was corroborated by cross-sectional scanning electron microscopy (SEM) images of a neat CNC film and a CNC/GLU film with 54 wt% glucose (Figure 1f,g; cross-section of a CNC/GLU film with 45 wt% glucose in Figure S4, Supporting Information). These images do not only illustrate the increase in the pitch with glucose content, but also show variations within each sample, including the tilt of the helical axis (see arrows in Figure 1g).
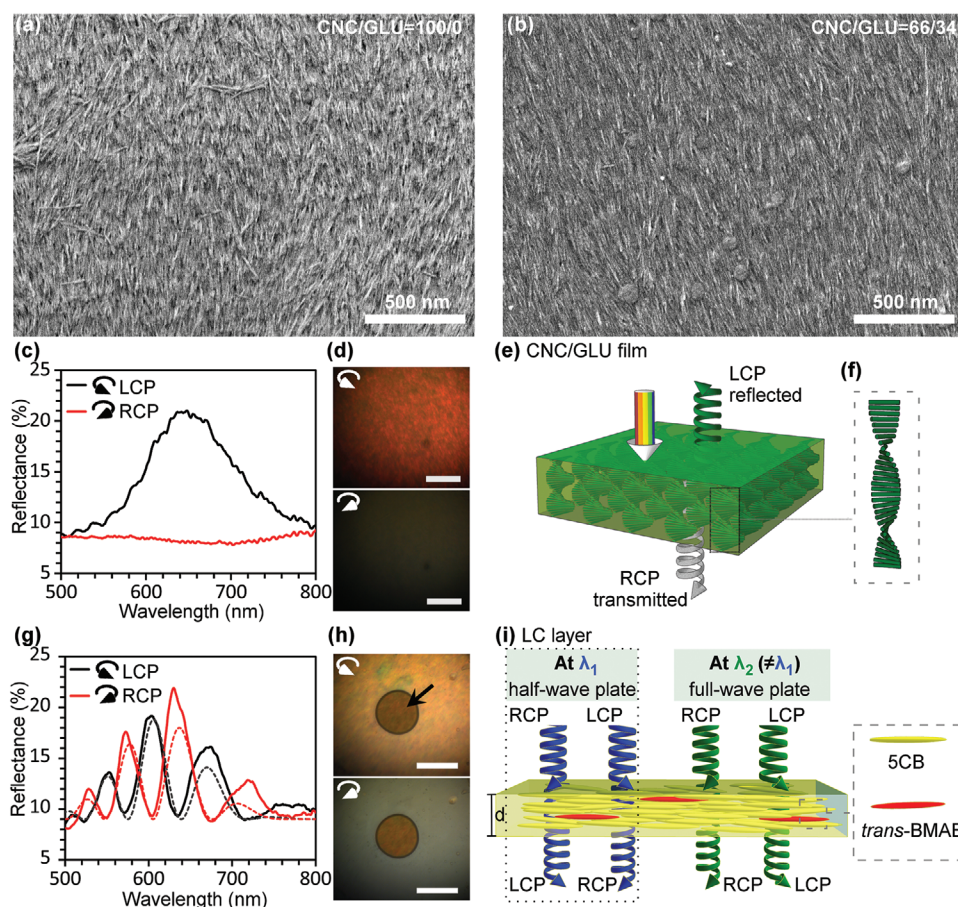
Figure 2. a,b) SEM images of film surfaces of a neat CNC film (a) and a nanocomposite film (CNC/GLU = 66/34) (b). The high level of CNC orientation (on the surface) is evident at this length-scale. c,d) Reflection of RCP and LCP light for a nanocomposite film (CNC/GLU = 39/61). Only LCP light is reflected whereas RCP light is transmitted, as illustrated in the simplified schematic in (e). f) A full-turn period (*p*) of CNCs. g,h) Reflection of incident RCP and LCP light for an LC droplet on top of a nanocomposite film (CNC/GLU = 39/61). Measurements performed close to the center of the LC droplet in (h). The black arrow points to the droplet. The dashed lines in (g) are calculated reflection spectra for incident RCP (red dashed line) and LCP (black dashed line) light. i) Schematic of the retardation behavior at different wavelengths (λ_1, λ_2) of a planarly aligned LC layer of thickness *d*. Scale bars: 200 µm (d) and 250 µm (h).

Figure 2a,b presents SEM images of a neat CNC film and a 66/34 CNC/GLU film, acquired from the top of the films at normal incidence (see Figure S5 of the Supporting Information for SEM image of the 52/48 CNC/GLU film). The images revealed clear alignment of the elongated CNCs along the film surface, extending significantly longer distances than the individual CNC length (150 ± 55 nm, assessed from transmission electron microscopy (TEM), *n* = 500, TEM images and histogram in Figure S6, Supporting Information). Lower magnification imaging also showed clear directional alignment (Figure S7, Supporting Information), while imaging the same film at positions further apart revealed that the alignment direction varied at the macroscopic scale (see Figure S8, Supporting Information). We hypothesize that the aligned CNCs may be used to (locally) orient adhering molecules on top of the film, such as liquid crystals (LCs). Indeed, the LC 4-cyano-4′-pentylbiphenyl (5CB) has previously been shown to planarly arrange itself at cellulose surfaces[16] and, furthermore, to follow the molecular orientation of the cellulose chains at the surface.[12,16] Our CNC/GLU films may therefore aid LCs deposited

on top to orient themselves along the film surface to form an optically birefringent layer.

To investigate this, we constructed hybrid cellulose–LC structures by drop-casting LC (a mixture containing 4.4 mol% 4-*n*-butyl-4′-methoxyazobenzene [BMAB] and 5CB) on top of CNC/GLU films (see the Experimental Section in the Supporting Information for details). This resulted in droplets of LCs on the films' surfaces. The LCs predominantly stayed on top of the CNC/GLU films, because we found no apparent swelling of the films, even after one month of storage. Swelling of the CNC/GLU film is expected to redshift the structural color of the film, but this was not observed. The results agree with contact angle measurements that confirmed only partial wetting of the surfaces of the CNC/GLU films (average contact angles = 30°–36°), results in Figure S9 of the Supporting Information. For optical measurements, the structure was further sandwiched between two glass substrates. Figure 2c,d shows reflection spectra and microscopy images for a bare CNC/GLU film illuminated by LCP or RCP light. In agreement with its chiral nematic structure (see schematic in Figure 2f) it reflected

only LCP light, while RCP light was transmitted (Figure 2c–f). The corresponding hybrid cellulose–LC nanophotonic structure showed a dramatically different optical response (Figure 2g,h). In regions containing the LC (black arrow in Figure 2h), it reflected both LCP and RCP light, but with inverse spectral profiles (Figure 2g). The combined LCP and RCP reflection resembled that of the bare CNC/GLU film (Figure S10, Supporting Information). While the bare film appeared dark in reflection when illuminated by RCP light, the hybrid structure displayed clear coloration for both LCP and RCP illumination. We attribute the modified optical response of the hybrid structure to the birefringent properties of the LC droplet, with parts of the liquid crystals being planarly aligned to the CNC/GLU surface (see illustration in Figure 2i). At the lateral boundaries of the droplet (air interface) and at the cover glass, the liquid crystal orientation is expected to be homeotropic[16] and unaligned (Figure S11, Supporting Information), respectively. The measurements on the LC droplets (Figure 2g and later) were always performed away from the lateral air interface. POM images, confirming the birefringent properties of LC droplets on top CNC/GLU films, are included in Figure S12 of the Supporting Information. The birefringence modifies the polarization of light interacting with the underlying CNC/GLU layer. The birefringent properties of the LC layer originate from its two orthogonal refractive indices (n_e, extraordinary and n_o, ordinary refractive index), which turn it into a retardation plate that modulates the relative optical phase as

$$\Delta\phi = \frac{2\pi(n_e - n_0)d}{\lambda} \tag{1}$$

where $\Delta\phi$ is the relative phase retardation between the two optical axes, d is the thickness, λ is the wavelength,[12] and $(n_e - n_o)$ is the birefringence of the LC. Similar LCs mixtures containing BMAB have shown birefringence of around 0.23, which we adopt in our calculations below.[17] For particular wavelengths (and assuming fixed d), the LC layer will act as a half-wave retardation plate ($\Delta\phi = \pi$, 3π, ...), such that incident LCP (RCP) light will have been converted to RCP (LCP) light when exiting on the other side of the LC layer (see Figure 2i). At these wavelengths (λ_1 in Figure 2i), incident RCP light will be reflected by the hybrid structure instead of incident LCP light, because light will have obtained opposite handedness before interacting with the cellulose film. At wavelengths where the LC layer instead acts as a full wave plate ($\Delta\phi = 2\pi$, 4π, ...), the polarization state will remain the same as that of the incident light, leading to preferential reflection of LCP light as for the bare CNC/GLU film (λ_2 in Figure 2i). This explains why the hybrid structure shows alternating reflection maxima and minima when illuminated by LCP or RCP light. The separation between neighboring maxima (or minima) corresponds to a phase shift of 2π, which together with Equation (1) (assuming a constant birefringence value) gives the effective birefringent LC layer thickness as

$$d = \left(\frac{1}{\lambda_1} - \frac{1}{\lambda_2}\right)^{-1} \cdot \frac{1}{n_e - n_0} \tag{2}$$

where λ_1 and λ_2 are the spectral positions of neighboring maxima (minima). Using values from Figure 2g, we determine

the effective birefringent LC thickness to be on the order of 25 µm. At wavelength between maxima and minima, the hybrid structure partially reflects both LCP and RCP incident light, in an oscillatory fashion and with inverse behavior for LCP and RCP light. The reason is that the phase shift for these wavelengths is not an integer of π ($\Delta\phi \neq \pi$, 2π, ...), which means that light exiting the LC layer and interacting with the CNC/GLU film will contain both LCP and RCP components. The fraction of LCP light exiting the LC layer (f_{LCP}) can be described by

$$f_{LCP} = \frac{1}{4}\left|1 - ie^{i\Delta\phi \pm \pi/2}\right|^2 \tag{3}$$

where the plus and minus $\pi/2$ correspond to the initial phase difference for incident LCP or RCP light, respectively (see the Supporting Information for details). Equation (3) describes how the birefringent LC layer modulates the reflection from the CNC/GLU film in an oscillatory manner, with out-of-phase behavior for incident LCP light and RCP light. To test this hypothesis, we approximate the LCP reflection from the pure CNC/GLU film as a Gaussian function (see details in the Supporting Information) and modulate this broad reflection using Equation (3) (together with Equation (1) to obtain $\Delta\phi$, using $d = 25$ µm and $n_e - n_o = 0.23$). The dashed lines in Figure 2g present the calculated results, which reproduces the experimental reflection features, including the inverse oscillations for incident LCP and RCP light.

An important feature of our LC mixture is that it makes the hybrid nanophotonic structure photoresponsive (**Figure 3**a). The reason is that the azobenzene dye (BMAB) can undergo a photoinduced isothermal phase transition through reversible photoisomerization.[18] In turn, this enables the BMAB to switch the host 5CB from its original nematic phase to an isotropic phase, which turns off the birefringence of the whole LC layer. The *cis*-BMAB, which creates the isotropic phase, can be formed by UV-light activation (see schematic in Figure 3a), whereas the recovery of the ordered nematic phase containing *trans*-BMAB, can be achieved by exposure to visible light (<550 nm, see Figure S14, Supporting Information) and/or by cooling past a specific transition temperature. As reported by Kurihara et al.,[18] the BMAB/5CB composition used in our study should turn back to its nematic phase from the isotropic phase at room temperature (≤27 °C).

Figure 3d shows the reflectance of a hybrid cellulose–LC structure prior to UV-light exposure, acquired close to the center region of the LC droplet (droplet marked with black arrow in Figure 3b). As discussed above, the structure provides structural reflection due to the CNC/GLU layer, with additional spectral oscillations induced by the birefringent LC. The sample was then removed from the microscope, exposed to UV-light, reinserted and monitored again on the same LC droplet (spot size was around 20 µm). Figures 3e and 3f show the optical response over time (t) for separate cycles measured with incident LCP and RCP light, respectively. We set $t = 0$ to the time at which the measurement spot had been located and started to be illuminated under the microscope. The initial reflectance for LCP and RCP light (shown at $t = 32$ s) strongly resembled that of the neat CNC/GLU film without the LC (Figure 3c), with only a broad peak centered at around 680 nm
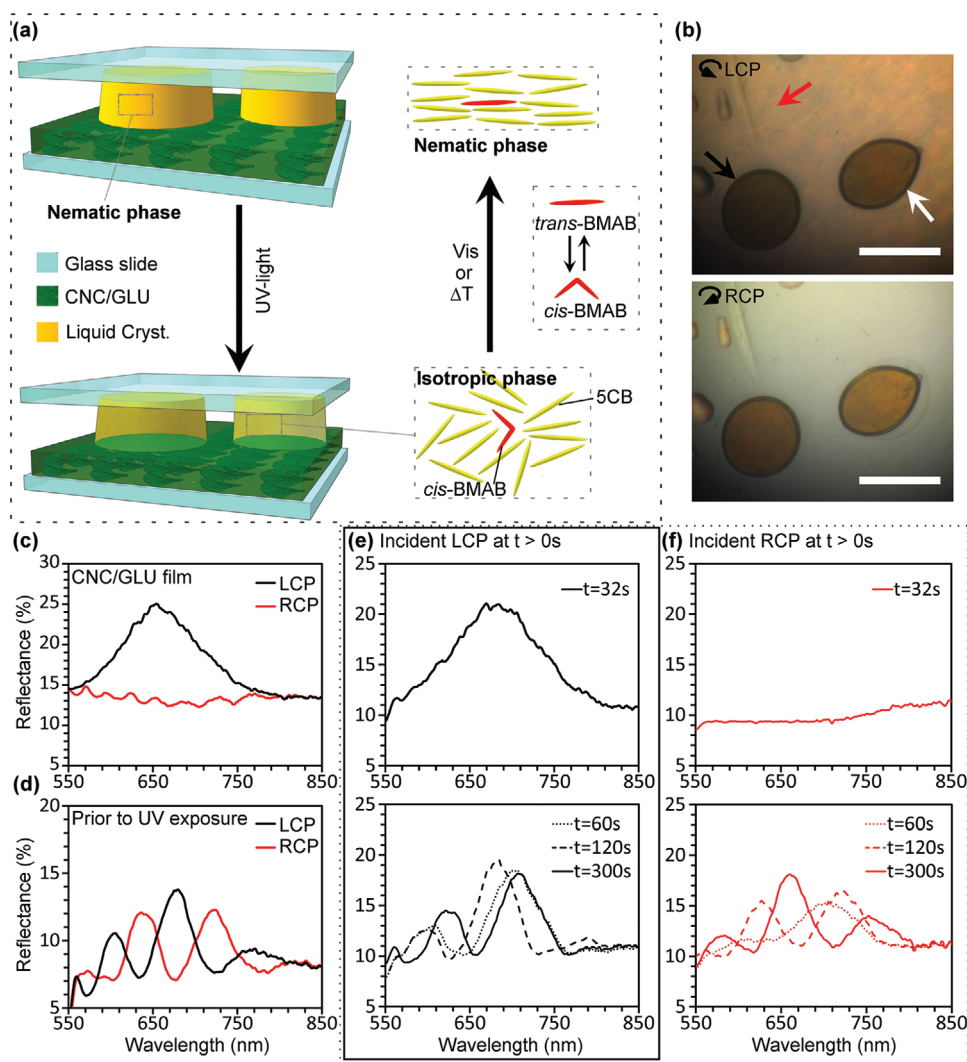
Figure 3. a) Simplified schematic of two LC droplets (BMAB/5CB mixture) on top of a CNC/GLU film. The LC droplets are in the nematic phase; then, after exposure to UV-light, the LCs convert to an isotropic phase. Exposure to visible light (vis) or cooling (ΔT) reverses the isotropic phase back to the ordered nematic phase. b) Optical polarized images in reflectance mode of two LC droplets (black and white arrows) residing on top of a CNC/GLU = 39/61 film (red arrow), when illuminated by incident LCP (top) or RCP (bottom) light. Scale bars: 250 µm. c) Reflectance results for the CNC/GLU film, see red arrow in (b). d) Reflectance results for a region with an LC droplet, measured close to the center of the droplet (the black arrow in (b) points to the droplet) prior to UV exposure (nematic phase). e–f) Reflectance results after UV exposure as a function of time (t =32, 60, 120, and 300 s) for incident LCP (e) or RCP (f) light. Measurements were performed on the same droplet as in (d). At t = 32 s, the LC is in the isotropic state and with time a gradual reversal back to the nematic phase is observed (steady state at 300 s).

for LCP light. This result confirms that the UV exposure successfully switched the LC molecules to a nonbirefringent isotropic state. Interestingly, the reflectance then evolved over time, with gradual reappearance of the spectral oscillations for both LCP and RCP light (see spectra at t = 60, 120, and 300 s (steady state)). This result implies that the BMAB isomerized from the *cis*- to the *trans*-form, which gradually reorganised the LC layer back to the more ordered nematic birefringent phase (illustrated in Figure 3a). The relatively fast switching to the *trans*-BMAB is attributed to a combination of temperature (experiments performed at room temperature) and light exposure. Although the multiple interference peaks reappeared over time, we note that the pattern at steady state did not fully match the spectra recorded prior to UV exposure (Figure 3d). This is

likely due to measuring at slightly different positions on the LC droplet (droplet marked with black arrow, Figure 3b), and there may also be small variations in the birefringence before and after the UV treatment procedure.

Figure 1c–e showed that each CNC/GLU film contained domains that reflected different colors, in agreement with relatively broad reflectance peaks. Combined with the LC layer, these different color domains within the same CNC/GLU film can selectively be reflected by altering the handedness of the incident circularly polarized light. Effectively, the LC-induced modulations of the original broad reflectance peak modify the perceived reflected colors of the nanocomposite structure. The color can be enhanced due to peak narrowing or it can change appearance more drastically if the oscillations suppress
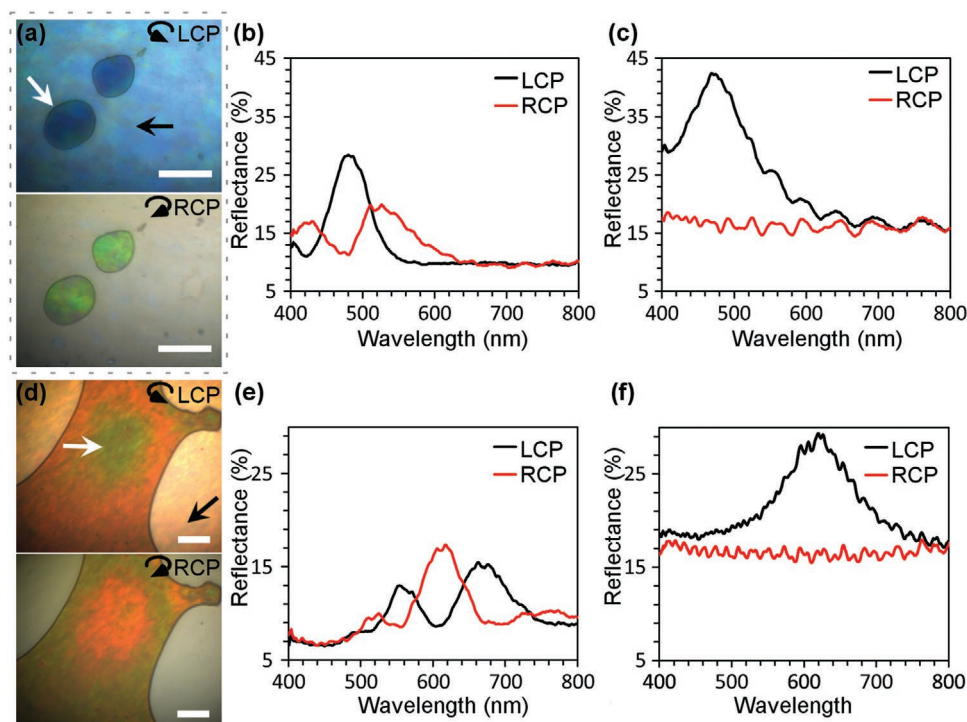
**ADVANCED
SCIENCE NEWS**

www.advancedsciencenews.com

**ADVANCED
MATERIALS**

www.advmat.de

Figure 4. Selective reflection of colors. a,d) Optical polarized images in reflectance mode of LC droplets (white arrows, BMAB in 5CB) residing on top of films (black arrows) with CNC/GLU compositions of 55/45 (a) and 39/61 (d). b,e) The reflectance spectra from the LC phase in, respectively, (a) and (d). The white arrows in (a) and (d) point to the LC droplet and measurement area, respectively. Measurements were acquired close to the center of the droplet to avoid artifacts from the droplet edges. c,f) The reflectance spectra from the bare CNC/GLU films in, respectively, (a) and (d). The black arrows in (a) and (d) point to the measurement areas on the bare CNC/GLU films. Scale bars: 150 µm.

reflection at the original peak wavelength of the CNC/CLU structure. We further note that the dominant reflectance peaks in LCP and RCP for the same structure can be quite far apart (≈50 nm), see Figure 3d. As a result, the cellulose–LC structure can provide different colors in reflection by switching between LCP and RCP illumination. To further exploit and demonstrate this property, LC droplets were created on top of CNC/GLU films of different original colors, and illuminated by RCP and LCP light. **Figure 4**a–c shows the results for a film that was blue for LCP illumination without the LC layer (CNC/GLU = 55/45). Notably, the color remained blue but became more distinct on regions with the LC layer (indicated by the white arrow) compared with regions only containing the bare film (black arrow). This is due to suppression of LCP reflection on both sides of the main reflection peak, which therefore became narrower (compare the black solid lines in Figure 4b,c). For RCP light, the same LC-containing region instead produced a clear green structural color. Comparing spectra on regions with and without the LC verifies that the spectral oscillations here suppressed the main blue reflection of the CNC/GLU film, resulting in the structure changing color from blue to green. This means that the reflected color could be altered between blue and green by simply switching polarization state of the incident light.

Figure 4d,f show the results for a red film (CNC/GLU = 39/61), for which the color could instead be changed between orange and yellowish green on LC-containing regions. At the measured position (marked by the white arrow), the sample produced yellowish green reflected color when illuminated by LCP light, while the bare film produced a vague red/orange reflection for LCP light (marked by the black arrow). The result agrees with the LC-induced spectral oscillations forming a reflection minimum close to the wavelength of the original peak position of the bare film (compare the black lines in Figure 4e,f). By contrast, RCP illumination showed a reflectance maximum at the same wavelength, resulting in orange color but more distinct compared with the bare CNC/GLU film illuminated by LCP light. For a given polarization state, we further note that the dominant reflected color varied within the same LC-containing region for this sample (Figure 4d). This is likely due to spatial variations in LC thickness and/or birefringence, which created an effective lateral modulation of the LC-induced phase shift.

3. Conclusion

We have presented a nanophotonic system with polarization and photoresponsive structural colors. Chiral self-assembled all-saccharide films provided a broad structural reflection peak for LCP light, with tailored resonance wavelengths across the visible spectral range via the glucose content. The optical response was then modulated by an overlaying birefringent LC layer, which induced spectral oscillations with inverse patterns for incident LCP and RCP light. The birefringent behavior of the LC layer implies that the LC molecules interacted with the

**ADVANCED
SCIENCE NEWS**

www.advancedsciencenews.com

**ADVANCED
MATERIALS**

www.advmat.de

cellulose and directionally aligned along the CNC surface. As a result of the LC-induced modulations, the reflected color of the nanophotonic structure could be controlled via the polarization state of the illumination (LCP or RCP light). We further demonstrated that the LC-induced modulations could be temporarily turned off by UV light exposure, which switched the LC layer into a nonbirefringent isotropic state. The presented structure resembles, to some extent, the many examples of light-responsive materials found in nature, which change their reflected colors in response to specific light stimuli. Examples include species such as small marine crustaceans, copepods, and beetles (*Plusiotis resplendens*).[12,19]

The straightforward production of materials with the ability to control their reflected color, as reported in this work, opens new avenues for cellulose-based nanophotonic materials, including systems that are capable of complex adaptive color switching in response to light changes.

Supporting Information

Supporting Information is available from the Wiley Online Library or from the author.

Acknowledgements

Conflict of Interest

The authors declare no conflict of interest.

Data Availability Statement

The data that support the findings of this study are available from the corresponding author upon reasonable request.

Keywords

[1] E. Moyroud, T. Wenzel, R. Middleton, P. J. Rudall, H. Banks, A. Reed, G. Mellers, P. Killoran, M. M. Westwood, U. Steiner, S. Vignolini, B. J. Glover, *Nature* **2017**, *550*, 469.

[2] R. Hamidjaja, J. Capoulade, L. Catón, C. J. Ingham, *ISME J.* **2020**, *14*, 2890.

[3] A. Sweeney, C. Jiggins, S. Johnsen, *Nature* **2003**, *423*, 31.

[4] M. Jacobs, M. Lopez-Garcia, O. P. Phrathep, T. Lawson, R. Oulton, H. M. Whitney, *Nat. Plants* **2016**, *2*, 16162.

[5] a) R. M. Graham, D. W. Lee, K. Norstog, *Am. J. Bot.* **1993**, *80*, 198; b) S. Vignolini, P. J. Rudall, A. V. Rowland, A. Reed, E. Moyroud, R. B. Faden, J. J. Baumberg, B. J. Glover, U. Steiner, *Proc. Natl. Acad. Sci. USA* **2012**, *109*, 15712.

[6] G. Guidetti, Y. Wang, F. G. Omenetto, *Nanophotonics* **2021**, *10*, 137.

[7] a) R. Bardet, F. Roussel, S. Coindeau, N. Belgacem, J. Bras, *Carbohydr. Polym.* **2015**, *122*, 367; b) R. Xiong, S. Yu, S. Kang, K. M. Adstedt, D. Nepal, T. J. Bunning, V. V. Tsukruk, *Adv. Mater.* **2020**, *32*, 1905600; c) Y. Yang, X. Wang, H. Huang, S. Cui, Y. Chen, X. Wang, K. Zhang, *Adv. Opt. Mater.* **2020**, *8*, 2000547.

[8] J. F. Revol, H. Bradford, J. Giasson, R. H. Marchessault, D. G. Gray, *Int. J. Biol. Macromol.* **1992**, *14*, 170.

[9] a) R. Bardet, N. Belgacem, J. Bras, *ACS Appl. Mater. Interfaces* **2015**, *7*, 4010; b) K. E. Shopsowitz, W. Y. Hamad, M. J. MacLachlan, *J. Am. Chem. Soc.* **2012**, *134*, 867; c) G. Guidetti, S. Atifi, S. Vignolini, W. Y. Hamad, *Adv. Mater.* **2016**, *28*, 10042; d) K. Yao, Q. Meng, V. Bulone, Q. Zhou, *Adv. Mater.* **2017**, *29*, 1701323; e) A. Querejeta-Fernández, G. Chauve, M. Methot, J. Bouchard, E. Kumacheva, *J. Am. Chem. Soc.* **2014**, *136*, 4788; f) J. He, K. Bian, N. Li, G. Piao, *J. Mater. Chem. C* **2019**, *7*, 9278; g) D. Qu, G. Chu, P. Martin, G. Vasilyev, R. Vilensky, E. Zussman, *ACS Appl. Mater. Interfaces* **2019**, *11*, 40443; h) J. Guo, B. Haehnle, D. Hoenders, G. Creusen, D. Jiao, A. J. C. Kuehne, A. Walther, *Adv. Mater.* **2020**, *32*, 2002332; i) H. Wan, X. Li, L. Zhang, X. Li, P. Liu, Z. Jiang, Z.-Z. Yu, *ACS Appl. Mater. Interfaces* **2018**, *10*, 5918; j) M. Xu, X. Wu, Y. Yang, C. Ma, W. Li, H. Yu, Z. Chen, J. Li, K. Zhang, S. Liu, *ACS Nano* **2020**, *14*, 11130; k) P. Grey, S. N. Fernandes, D. Gaspar, E. Fortunato, R. Martins, M. H. Godinho, L. Pereira, *Adv. Funct. Mater.* **2019**, *29*, 1805279.

[10] D. Qu, H. Zheng, H. Jiang, Y. Xu, Z. Tang, *Adv. Opt. Mater.* **2019**, *7*, 1801395.

[11] a) J. A. Kelly, M. Yu, W. Y. Hamad, M. J. MacLachlan, *Adv. Opt. Mater.* **2013**, *1*, 295; b) O. Kose, A. Tran, L. Lewis, W. Y. Hamad, M. J. MacLachlan, *Nat. Commun.* **2019**, *10*, 510; c) C. E. Boott, A. Tran, W. Y. Hamad, M. J. MacLachlan, *Angew. Chem., Int. Ed.* **2020**, *59*, 226.

[12] S. N. Fernandes, P. L. Almeida, N. Monge, L. E. Aguirre, D. Reis, C. L. P. de Oliveira, A. M. F. Neto, P. Pieranski, M. H. Godinho, *Adv. Mater.* **2017**, *29*, 1603560.

[13] B. Frka-Petesic, J. A. Kelly, G. Jacucci, G. Guidetti, G. Kamita, N. P. Crossette, W. Y. Hamad, M. J. MacLachlan, S. Vignolini, *Adv. Mater.* **2020**, *32*, 1906889.

[14] A. G. Dumanli, H. M. van der Kooij, G. Kamita, E. Reisner, J. J. Baumberg, U. Steiner, S. Vignolini, *ACS Appl. Mater. Interfaces* **2014**, *6*, 12302.

[15] D. G. Gray, X. Y. Mu, *Materials* **2015**, *8*, 7873.

[16] L. E. Aguirre, A. de Oliveira, D. Seč, S. Čopar, P. L. Almeida, M. Ravnik, M. H. Godinho, S. Žumer, *Proc. Natl. Acad. Sci. USA* **2016**, *113*, 1174.

[17] a) Y. J. Liu, G. Y. Si, E. S. P. Leong, N. Xiang, A. J. Danner, J. H. Teng, *Adv. Mater.* **2012**, *24*, OP131; b) Y. Zhao, Q. Hao, Y. Ma, M. Lu, B. Zhang, M. Lapsley, I.-C. Khoo, T. J. Huang, *Appl. Phys. Lett.* **2012**, *100*, 053119.

[18] S. Kurihara, K. Ohta, T. Oda, R. Izumi, Y. Kuwahara, T. Ogata, S.-N. Kim, *Sci. Rep.* **2013**, *3*, 2167.

[19] M. E. McConney, M. Rumi, N. P. Godman, U. N. Tohgha, T. J. Bunning, *Adv. Opt. Mater.* **2019**, *7*, 1900429.